

Random matrix model of Kolmogorov-Zakharov turbulence

Klaus M. Frahm  and Dima L. Shepelyansky 

Laboratoire de Physique Théorique, IRSAMC, Université de Toulouse, CNRS, UPS, 31062 Toulouse, France



(Received 21 January 2024; accepted 8 March 2024; published 1 April 2024)

We introduce and study a random matrix model of Kolmogorov-Zakharov turbulence in a nonlinear purely dynamical finite-size system with many degrees of freedom. For the case of a direct cascade, the energy and norm pumping takes place at low energy scales with absorption at high energies. For a pumping strength above a certain chaos border, a global chaotic attractor appears with a stationary energy flow through a Hamiltonian inertial energy interval. In this regime, the steady-state norm distribution is described by an algebraic decay with an exponent in agreement with the Kolmogorov-Zakharov theory. Below the chaos border, the system is located in the quasi-integrable regime similar to the Kolmogorov-Arnold-Moser theory and the turbulence is suppressed. For the inverse cascade, the system rapidly enters a strongly nonlinear regime where the weak turbulence description is invalid. We argue that such a dynamical turbulence is generic, showing that it is present in other lattice models with disorder and Anderson localization. We point out that such dynamical models can be realized in multimode optical fibers.

DOI: [10.1103/PhysRevE.109.044201](https://doi.org/10.1103/PhysRevE.109.044201)

I. INTRODUCTION

The Kolmogorov concept of turbulence [1,2] assumes emergence of energy flow through an inertial interval from large spatial scales, with an external pumping, to small scales where energy is absorbed by dissipation. The scaling arguments lead to the appearance of a power-law energy distribution over wave modes for hydrodynamics turbulence [1,2]. This concept was generalized and extended to weak wave turbulence, based on diagrammatic techniques and the kinetic equation, indeed showing the emergence of power-law distributions for various types of weakly interacting nonlinear waves [3–7]. This theory became known as Kolmogorov-Zakharov (KZ) turbulence (or spectra) [5–7]. In spite of various successful confirmations of this theory in experiments and numerical simulations (see, e.g., [5–7]), it is still based on a fundamental hypothesis directly stated in the seminal work of Zakharov and Filonenko [3]: “In the theory of weak turbulence nonlinearity of waves is assumed to be small; this enables us, using the hypothesis of the random nature of the phase of individual waves, to obtain the kinetic equation for the mean square of the wave amplitudes.” Nevertheless, the dynamical equations for waves do not involve random phase approximation (RPA) and hence the validity for the whole concept of energy flow from large to small scales remains open.

Indeed, a flow through an inertial interval is Hamiltonian and it is well known that in nonlinear systems with weak nonlinearity, the Kolmogorov-Arnold-Moser (KAM) theory guarantees that the main part of the system phase space remains integrable and nonchaotic in the limit of very weak nonlinearity (see, e.g., [8,9]; note that KAM theory is valid in the absence of exact resonances, as discussed below). More physical analysis of nonlinear dynamical Hamiltonian systems also shows the existence of a chaos border below which the phase space contains mainly an integrable dynamics opposite to the turbulent one [10,11].

Therefore, to better understand the fundamental aspects of KZ turbulence (KZT), here we introduce and study a different random matrix model (RMM) of KZT described only by dynamical equations of motion. This model is an extension of the nonlinear random matrix model (NLIRM) recently introduced in [12] and which describes a dynamical system of linear oscillators coupled by a random matrix combined with a nonlinear interaction between oscillators in the form of a quartic nonlinearity corresponding to four-wave interactions in nonlinear media. This system is Hamiltonian with two conserved integrals of motion.

Random matrix theory (RMT), introduced by Wigner [13], describes generic spectral properties of complex nuclei, atoms, and molecules [14,15], and systems of quantum chaos [16,17]. In particular, RMT eigenstates are ergodic and uniformly distributed on the N -dimensional unit sphere, and the level spacing statistics is characterized by the universal RMT distribution.

These ergodic RMT eigenstates provide nonlinear long-range couplings between the oscillator modes in the NLIRM which leads, for a rather weak nonlinearity (but still above a certain chaos border), to dynamical thermalization according to classical statistical mechanics [18] with a steady-state thermal distribution characterized by energy equipartition [12].

In particular, in the NLIRM, the dynamical thermalization appears in the absence of any thermal bath. This is possible because, due to the ergodic RMT eigenstates, the NLIRM allows one to avoid specific features of nonlinear oscillator models which can be close to certain completely integrable systems which makes it difficult to achieve dynamical thermalization. Indeed, this happened for the seminal Fermi-Pasta-Ulam (FPU) problem [19], which appeared to be close to completely integrable soliton systems such as the Korteweg-De Vries equation [20], the nonlinear Schrödinger equation [21], or the Toda lattice [22].

For these reasons, we think that the NLIRM [12] can be used as a basis for dynamical modeling of KZ turbulence. For this, we extend the NLIRM by additional terms describing pumping with nonlinear saturation at low energies and dissipation at high energies. The form of such pumping is rather standard, being used in systems of fluid mechanics [23] and models of random lasing (see, e.g., [24,25]). We call this extended model the RMM of KZ turbulence.

Our studies for this model show that the direct cascade in this system is described by an algebraic decay of the KZ turbulent spectrum [4] with an exponent being close to the expected theoretical value, if the pumping strength is above a certain chaos border, while below this border the flow to high energies is suppressed, in analogy with KAM theory. The properties of the inverse cascade are more complex, as we discuss below.

The paper is organized as follows: in Sec. II, we remind the reader of the NLIRM of [12] and generalize it to include pumping and dissipation at certain energy modes. Section III provides some theoretical conclusions based on the KZ theory of [4] for our model. Section IV presents and analyzes the numerical results for three different cases of a direct and an inverse cascade of the RMM and also the direct cascade for a variant with short-range oscillator couplings similar to the Anderson one-dimensional (1D) model, and Sec. V provides the final discussion.

II. MODEL DESCRIPTION

In the absence of pumping and dissipation, the RMM of KZT is reduced to the NLIRM model studied in [12], with the time evolution described by

$$i\hbar \frac{\partial \psi_n(t)}{\partial t} = \sum_{n'=1}^N H_{n,n'} \psi_{n'}(t) + \beta |\psi_n(t)|^2 \psi_n(t). \quad (1)$$

Here, $H_{n,n'}$ are elements of an RMT matrix \hat{H} of size N generated from the Gaussian orthogonal ensemble (GOE) [14]; they have zero mean and variance $\langle H_{n,n'}^2 \rangle = (1 + \delta_{n,n'}) / [4(N + 1)]$. The averaged density of states is described by the semicircle law $dm/dE = \frac{2N}{\pi} \sqrt{1 - E^2}$, with typical eigenvalues in the interval $E_m \in [-1, 1]$ (we use dimensionless units with $\hbar = 1$). Here, β is a dimensionless constant characterizing the nonlinear interaction strength in the original basis n . For most energies close to the band center, we can consider that the eigenenergies E_m are changing approximately linearly with m [$E_m \approx \pi(m - N/2)/(2N)$; $1 \leq m \leq N$], however, keeping in mind that at the spectrum boundaries, the density of states drops significantly.

We denote by $\phi_n^{(m)}$ the eigenmodes of \hat{H} at eigenenergies E_m . They are ergodic with a uniform distribution on the N -dimensional unit sphere [14] for fixed m and mutually orthogonal between different m . The time evolution of the system wave function can also be expressed in the basis of eigenmodes $\phi_n^{(m)}$ by $\psi_n(t) = \sum_{m=1}^N C_m(t) \phi_n^{(m)}$ (see below). Here the coefficients $C_m(t)$ give the occupation probability $\rho_m = \langle |C_m(t)|^2 \rangle$, where brackets denote some long-time or ensemble average (see below). The time evolution (1) has two integrals of motion. They are the (squared) norm $\sum_n |\psi_n(t)|^2 = 1$ and total energy

$E = \sum_n \langle \psi_n(t) | \hat{H} | \psi_n(t) \rangle + (\beta/2) |\psi_n(t)|^4$. At $\beta = 0$, the model (1) can be viewed as a quantum system or as a classical system of coupled linear oscillators whose Hamiltonian in the basis of oscillator eigenmodes is $\mathcal{H} = \sum E_m C_m^*(t) C_m(t)$, with C_m, C_m^* being a pair of conjugated variables; E_m plays the role of oscillator frequencies.

Due to the nonlinear term, the eigenmodes are getting a nonlinear frequency shift of $\delta\omega \sim \beta |\psi_n|^2 \sim \beta/N$. In [26–28], it was argued that a developed chaos takes place when this shift $\delta\omega$ becomes comparable to a typical energy spacing between energies (or frequencies) of the linear system $\Delta\omega \sim 1/N$. Thus, $\delta\omega > \Delta\omega$ implies chaos with the chaos border $\beta_c = \text{const} \sim 1$ being independent of system size N . Thus, above chaos border $\beta > \beta_c$, a moderate nonlinearity destroys KAM integrability, leading to chaotic dynamics with a positive maximal Lyapunov exponent λ and dynamical thermalization, as shown in [12].

The steady-state thermal distribution of probabilities ρ_m has the standard form corresponding to the results of statistical mechanics [18],

$$\rho_m = \rho_{\text{EQ}}(E_m) \equiv \frac{T}{E_m - \mu}, \quad (2)$$

corresponding to the equipartition of energies $\langle (E_m - \mu) |C_m|^2 \rangle = (E_m - \mu) \rho_m = T$, where T is the system temperature, and $\mu(T)$ is the chemical potential dependent on temperature. These two parameters are determined from the total norm $\kappa \equiv \sum_m \rho_m = 1$ and the energy E , which are conserved integrals of motion, by the implicit equations $\kappa = \sum_m \rho_{\text{EQ}}(E_m) = 1$ and $\sum_m E_m \rho_{\text{EQ}}(E_m) = E$ (for E , we assume the case of a weak or moderate nonlinearity which provides only a weak contribution to the total energy). The entropy S of the system is given by the usual relation [18] $S = -\sum_m \rho_m \ln \rho_m$, with the implicit theoretical dependencies on temperature $E(T)$, $S(T)$, and $\mu(T)$ (see details in [12]). We note that a random matrix model similar to those considered in [12] and in (1) was considered in [29], but a detailed study of dynamical thermalization was not presented there.

It is interesting to note that the dynamical thermal, or Rayleigh-Jeans, distribution (2) has been observed in optical multimode fibers [30–34] (there a length z along the fiber corresponds to the time variable discussed here). At low temperatures T , the thermal distribution (2) has maximal probabilities at low energy modes that was called self-cleaning in fibers. At the same time, we note that in all fiber experiments [30–34], the dynamics of rays in the linear system (at zero nonlinear term) is always integrable, usually corresponding to a case of two-dimensional oscillator (2D) potential with equal frequencies. The linear mode frequencies (or quantum energy levels) of such a 2D oscillator are degenerate and formally the KAM theory is not valid in such a situation. In particular, it was shown that for three oscillators

¹For simplicity of notation, we use the notation *norm* for the quantity κ even though it is a certain time averaged norm $|C_m(t)|^2$ of the quantum state with amplitudes $C_m(t)$. Actually, κ is mathematically the 1-norm of the vector with coefficients ρ_m . Furthermore, we denote as *norm distribution* the dependence of ρ_m on energies E_m , in particular for the cases where $\kappa \neq 1$.

with equal frequencies, about half of the phase space is chaotic even at arbitrary small nonlinear coupling [26,35]. A similar situation also appears for equidistant mode frequencies coupled by a nonlinear interaction in the FPU problem [36]. Therefore, the situation of fiber experiments [30–34] does not directly correspond to the case of RMT mode frequencies or a case when a linear system belongs to the domain of quantum chaos [16,17] which has spectral properties being close to those of RMT. We discuss relations between the NLIRM model (1) with multimode fiber experiments below in more detail.

To model the KZ turbulence, we generalize (1) by adding terms for pumping and dissipation (absorption) at specific energy eigenmodes. For this, it is more convenient to rewrite the time evolution equation (1) by replacing ψ_n with the amplitudes $C_m(t)$ obtained from the expansion of ψ_n in the basis of the linear eigenmodes $\phi_n^{(m)}$. This provides the following generalized NLIRM model with pumping and dissipation:

$$i \frac{\partial C_m}{\partial t} = E_m C_m + i(\gamma_m - \sigma_m |C_m|^2) C_m + \beta \sum_{m_1 m_2 m_3} V_{m m_1 m_2 m_3} C_{m_1} C_{m_2}^* C_{m_3}. \quad (3)$$

The Hamiltonian case (1) is a special case of (3) with $\gamma_m = \sigma_m = 0$ (taking into account the linear transformation $\psi_n \rightarrow C_m$). In (3), the transitions between linear eigenmodes appear only due to the nonlinear β term and the transition matrix elements are $V_{m m_1 m_2 m_3} = \sum_n \phi_n^{(m)*} \phi_n^{(m_1)} \phi_n^{(m_2)*} \phi_n^{(m_3)} \sim 1/N^{3/2}$ [27] due to the sum of N random terms with typical size N^{-2} since, according to RMT [14], $\phi_n^{(m)} \sim N^{-1/2}$. Furthermore, assuming “random” C_m values of comparable size, $C_m \sim C$, the β term in (3) has an overall size $\sim \beta C^3$ (sum of about N^3 random terms of typical size $V \sim N^{-3/2}$).

In (3), nonzero values of $\gamma_m > 0$, $\sigma_m > 0$ correspond to pumping modes or $\gamma_m < 0$, $\sigma_m = 0$ to dissipation modes. To obtain the energy flow of a direct cascade from low to high energy modes m , we choose for pumping $\gamma_m = \gamma > 0$ for the four lowest energy modes at $m = 1, 2, 3, 4$ with corresponding saturation coefficients $\sigma_m = \sigma > 0$ and for dissipation $\gamma_m = -\gamma < 0$, $\sigma_m = 0$ for the four highest energy modes with $m = N, N - 1, N - 2, N - 3$. For all other m values, we choose $\gamma_m = \sigma_m = 0$. Here, γ and σ are two parameters of our model and, in most cases, we choose $\gamma = \sigma = 0.01$.

To model an inverse cascade, we also consider the case when pumping is done at four m values close to a certain pumping mode m_0 in mode space (with $m = m_0 - 2, \dots, m_0 + 1$) and dissipation at system boundaries ($m = 1, \dots, 4$ and $m = N - 3, \dots, 1$).

In this way, we obtain a purely dynamical random matrix model of KZ turbulence described by Eq. (3), which we call RMM of KZT. This can be considered as a model of dynamical turbulence without any couplings to an external thermal bath or external noise.

We mention that in the absence of the nonlinear coupling, i.e., if $\beta = 0$, the amplitudes $C_m(t)$ decouple and (3) allows for the analytical solution

$$C_m(t) = \frac{C_m(0) e^{-iE_m t}}{\sqrt{D_m + (1 - D_m) e^{-2\gamma_m t}}}, \quad D_m \equiv |C_m(0)|^2 \frac{\sigma_m}{\gamma_m}, \quad (4)$$

which simplifies to $C_m(t) = C_m(0) e^{(-iE_m + \gamma_m)t}$ if $\sigma_m = 0$. For the pumping case with $\gamma_m = \gamma > 0$ and $\sigma_m = \sigma > 0$, this solution provides $|C_m(t)| \rightarrow C_{\text{sat}} \equiv \sqrt{\gamma/\sigma}$ for $t \rightarrow \infty$, with C_{sat} being the saturation value of the amplitudes. Initial small amplitudes $|C_m(0)| \ll C_{\text{sat}}$ grow for short timescales as $|C_m(t)| \sim e^{\gamma t}$ and large initial amplitudes $|C_m(0)| \gg C_{\text{sat}}$ decay as $|C_m(t)| \sim C_{\text{sat}}/\sqrt{2\gamma t}$ for (very) short timescales and, in both cases, they saturate at C_{sat} with $||C_m(t) - C_{\text{sat}}| \sim e^{-2\gamma t}$ for longer timescales. For $\beta = 0$ and dissipation modes, there is a simple exponential decay $|C_m(t)| \sim e^{-\gamma t}$. In all cases, the phase $C_m(t)/|C_m(t)| = e^{-iE_m t}$ behaves as in the quantum or pure oscillator case.

It is interesting to note that in the limit of a strong β term, or $E_m = 0$, and $\gamma_m = \sigma_m = 0$, Eq. (3) is similar to the random coupling model of turbulence that can be considered as a classical Sachdev-Ye-Kitaev model [37].

III. THEORETICAL KZ SPECTRA FOR RMM

In the theory of KZ spectra, it is usually assumed that the frequency ω spectrum of linear waves is an algebraic function of the wave vector k with $\omega(k) \propto k^\alpha$; the four-wave interaction matrix elements are also algebraic functions of k with an exponent χ ($V \propto k^\chi$) and the system dimension is d . Then the stationary solution of the direct cascade of energy flow from low to high energies also has an algebraic solution, with the density in k space being ([4]; see Eq. (3.1.10a) there)

$$\rho_k \propto k^{-s_0}, \quad s_0 = 2\chi/3 + d. \quad (5)$$

In our case for RMM, the wave vector k corresponds to the eigenmode index m and we have $d = 1$, $\chi = 0$ [matrix elements V in (3) are independent of m] with $\alpha \approx 1$ (assuming a constant density of states for the center part of the semicircle law, we have approximately $E_m + 1 \propto m$ with an energy shift counted from the lower energy border). Hence, the theoretical steady-state density for RMM is

$$\rho_m \propto 1/(E_m + 1)^{-s_0}, \quad s_0 = 1. \quad (6)$$

For the inverse cascade of norm flow in RMM, we have, from [4] [see Eq. (3.1.10b) there],

$$\rho_m \propto (E_m + 1)^{-x_0}, \quad x_0 = 2\chi/3 + d - \alpha/3 = 2/3. \quad (7)$$

We perform, for RMM of KZT, a comparison of the above theoretical predictions with the results of the numerical simulations in the next section.

IV. NUMERICAL RESULTS FOR RMM OF KZT

The numerical integration of the time evolution described by Eq. (3) is done in the same way as described in [12] using a fourth-order integration method with a basic time step $\Delta t = 0.1$. In the absence of pumping and dissipation, the method conserves the symplectic symmetry and is also called “symplectic integrator.” In particular, in this case, the total norm $\kappa = \sum_m |C_m(t)|^2$ is conserved up to numerical precision and the classical energy is conserved numerically at a level of 10^{-8} . This integration method applies alternate small integration steps in the original lattice n basis (only using the nonlinear β term), followed by a small integration step of the other terms (obtained by putting $\beta = 0$) in the

linear eigenmode m basis of the random matrix \hat{H} . Between two steps, the linear transformation between $\psi_n \rightarrow C_m$ or its inverse transformation $C_m \rightarrow \psi_n$ is applied in order to switch back and forth from one to the other basis, and vice versa. The succession of the eight or six (using a certain symmetry optimization) individual integration time steps is carefully chosen as certain fractions of Δt such that the global precision of the method is fourth order, with a global error of $\sim(\Delta t)^4$ (see [12] and references therein for details).

In the presence of pumping and dissipation terms, the system described by (3) is no longer symplectic, but the numerical method can still directly be applied to this case using the analytical solution (4) for $\beta = 0$ for the integration steps in C_m representation and the overall precision is still $\sim(\Delta t)^4$.

These terms break norm and energy conservation, leading to turbulent energy and norm flows between energy scales which are at the basis of KZ spectra [4]. However, in-between pumping and dissipation, the dynamics (3) remains Hamiltonian, as is assumed in KZ theory.

A. Direct cascade of KZT

We start with the analysis of the direct energy cascade from low to high energies, where the pumping is done at the lowest linear energy modes $m = 1, \dots, 4$ and absorption (or dissipation) is done at the highest energy modes $m = N - 4, \dots, N$. We choose the initially populated modes at $m = 1, \dots, 8$ with random amplitudes $C_m(t=0)$ and a total norm $\kappa = \sum_m |C_m(0)|^2 = 0.01$. A small value of κ corresponds to an image of a calm sea surface with very weak wind modeled by pumping. The results for system sizes $N = 128, 256$, $\beta = 1$, $\gamma = \sigma = 0.01$ are presented in Fig. 1. They show that at large times $t = 2^{22}$, there is a convergence to a stationary norm distribution ρ_m which is approximately described by an algebraic decay of the norm population ρ_m with energy $E_m + 1$, counted from the spectrum border. The decay exponent s_0 , given by fit, decreases with an increase of the system size of $s_0 = 1.48; 1.24$ at $N = 128, 256$. The fit for the algebraic decay is done for the range $0.2 \leq E_m + 1 \leq 1.8$ to exclude the boundary effects of pumping and absorption. Indeed, at low values of m (or $E_m + 1$), the amplitudes $C_m(t)$ fluctuate around the saturation value (for $\beta = 0$) $C_m \approx C_{\text{sat}} = \sqrt{\gamma/\sigma} = 1$ corresponding to the regime when γ pumping is compensated by the nonlinear σ term. The total norm is $\kappa = 5.31$, showing that the largest fraction of norm is located on the pumping modes $m = 1, \dots, 4$ and a smaller norm fraction is transferred by a turbulent flow to high energies. At the boundary near $m = N$, the norm values ρ_m drop due to absorption.

We point out that the steady-state distributions ρ_m , shown in Fig. 1 for a specific random realization of RMT matrix $H_{n,n'}$ in (1), are qualitatively the same for other random realizations of $H_{n,n'}$. In Fig. 2, we show steady-state distributions ρ_m for 10 different realizations that have approximately the same shape with an average algebraic exponent $s_0 = 1.32 \pm 0.03$. The pumping region at $m = 1, \dots, 4$ contains the main fraction of the total norm κ and, depending on the disorder realization of $H_{n,n'}$ and E_m , there are considerable fluctuations of the numerical prefactor of the power law, while the shape of the algebraic decay of ρ_m at higher energies remains independent of disorder.

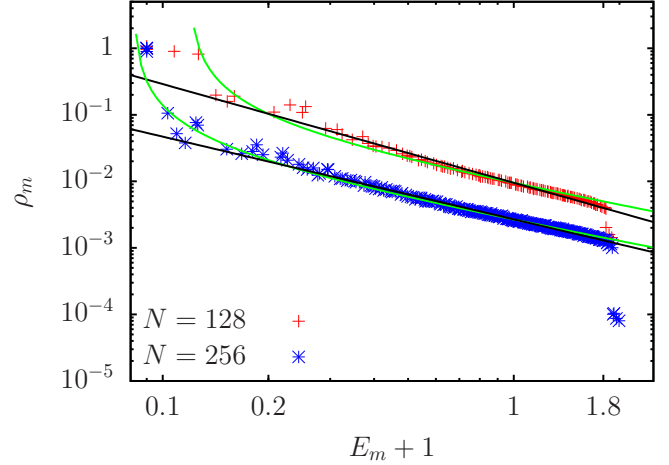


FIG. 1. Distribution ρ_m vs $E_m + 1$ in a double-logarithmic representation for $N = 128$ (red +) and $N = 256$ (blue *), $\gamma = \sigma = 0.01$, $\beta = 1$, pumping at $m = 1, \dots, 4$, and absorption at $m = N - 3, \dots, N$. The values of ρ_m have been obtained from the time average $\rho_m(t) = \langle |C_m(\tau)|^2 \rangle$ for $t/2 \leq \tau \leq t$ with $t = 2^{22}$. The initial condition corresponds to uniform random values $C_m(0)$ for $m = 1, \dots, 8$ and $C_m(0) = 0$ for $m > 8$, with initial squared norm $\sum_m |C_m(0)|^2 = 0.01$. Data points with $E_m + 1 < 0.09$ have been artificially moved to $E_m + 1 = 0.09$. The black straight lines show the power-law fit $\rho_m = A(1 + E_m)^{-s_0}$ using the fit range $0.2 \leq 1 + E_m \leq 1.8$ with $A = (9.52 \pm 0.10) \times 10^{-3}$, $s_0 = 1.48 \pm 0.02$ (for $N = 128$), and $A = (2.69 \pm 0.01) \times 10^{-3}$, $s_0 = 1.24 \pm 0.01$ (for $N = 256$). The average total norm is $\kappa = \sum_m \rho_m = 6.25$ (for $N = 128$) and $\kappa = 5.31$ (for $N = 256$). The green curves show the theoretical equipartition distribution $\rho_{\text{EQ}}(E_m)$ of Eq. (2) obtained from a reduced spectrum $4 < m < N - 3$, excluding both pumping and dissipation modes with effective temperature $T = 8.40 \times 10^{-3}$ and chemical potential $\mu = -0.881$ (for $N = 128$) and $T = 2.45 \times 10^{-3}$, $\mu = -0.918$ (for $N = 256$; see text for details). The values of the reduced norm κ_r and reduced energy E_r used in Eq. (8) are $\kappa_r = 2.489$, $E_r = -1.185$ (for $N = 128$) and $\kappa_r = 1.417$, $E_r = -0.6930$ (for $N = 256$).

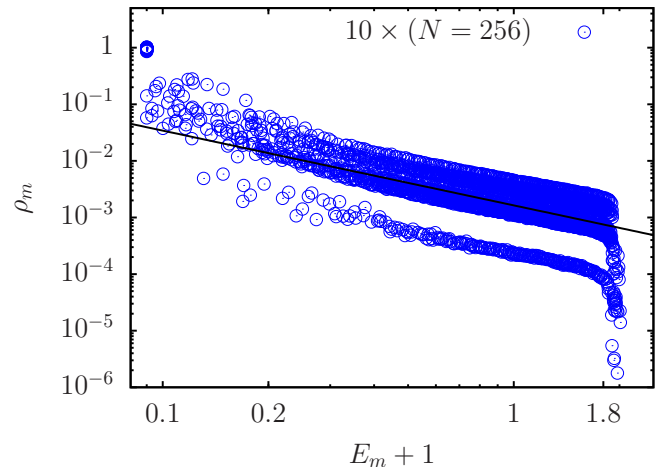


FIG. 2. Same as Fig. 1 for $N = 256$ and 10 different random matrix realizations \hat{H} (the other parameters are the same and blue \circ represent data points). The straight line shows the power-law fit $\rho_m = A(1 + E_m)^{-s_0}$ using the fit range $0.2 \leq 1 + E_m \leq 1.8$ and all data points for all 10 random matrix realizations with $A = (1.64 \pm 0.03) \times 10^{-3}$, $s_0 = 1.32 \pm 0.03$. The average norm is in the interval $4.18 \leq \kappa = \sum_m \rho_m \leq 6.57$ for the 10 random matrix realizations.

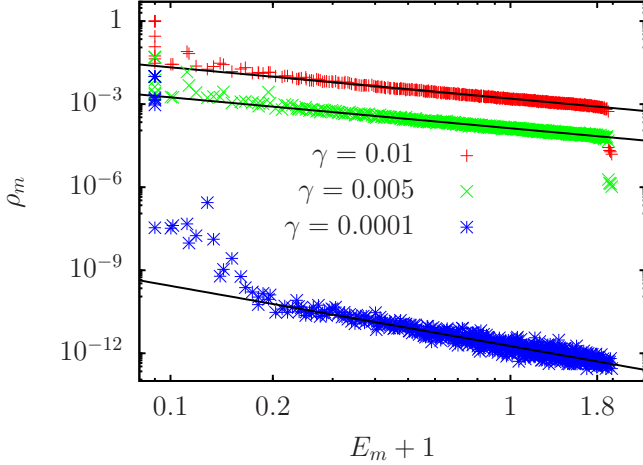


FIG. 3. Same as Fig. 1, but $N = 512$ and modified values $\gamma = 0.01$ (red +), $\gamma = 0.005$ (green \times and shifted down by a factor of 10 for better visibility), and $\gamma = 0.0001$ (blue $*$). (Values for $\beta = 1$, $\sigma = 0.01$, $t = 2^{22}$ modes for pumping and absorption and initial condition are unchanged with respect to Fig. 1.) The straight lines show the power-law fit $\rho_m = A(1 + E_m)^{-s_0}$ using the fit range $0.2 \leq 1 + E_m \leq 1.8$, with $A = (1.584 \pm 0.003) \times 10^{-3}$, $s_0 = 1.130 \pm 0.004$ (for $\gamma = 0.01$), $A = (1.343 \pm 0.004) \times 10^{-3}$, $s_0 = 1.117 \pm 0.005$ (for $\gamma = 0.005$), and $A = (1.82 \pm 0.03) \times 10^{-12}$, $s_0 = 2.17 \pm 0.03$ (for $\gamma = 0.0001$). The average total norm is $\kappa = 5.99$ (for $\gamma = 0.01$), 3.58 (for $\gamma = 0.005$), and 0.0455 (for $\gamma = 0.0001$).

The fit values of s_0 in Figs. 1 and 2 are somewhat higher than the theoretical value $s_0 = 1$ from (6). We attribute this to effects of finite system size N and to deviations from the assumed constant density of states at the boundary of the semicircle spectrum. Indeed, for the higher value $N = 512$ shown in Fig. 3, we obtain the exponent $s_0 = 1.130 \pm 0.004$ that is close to the theoretical KZT value $s_0 = 1$ of Eq. (6) [4].

One can also ask the question of how far the numerical results for Fig. 1 correspond to the statistical equipartition distribution (2). Obviously, the numerical values of ρ_m in Fig. 1 are significantly enhanced (reduced) for pumping (dissipation) modes m if compared to ρ_m for other close m nonpumping (nondissipation) modes, and also from a theoretical viewpoint, it is not reasonable to expect that Eq. (2) is valid for the full spectrum including pumping and dissipation modes. However, one may surmise that the long-time ($t = 2^{22}$) steady-state distribution for the reduced spectrum with $4 < m < N - 4$, excluding pumping and dissipation modes, approximately satisfies the statistical equipartition distribution (2). To verify this point, we have determined T and μ by the two implicit equations

$$\kappa_r = \sum'_m \rho_{\text{EQ}}(E_m), \quad E_r = \sum'_m E_m \rho_{\text{EQ}}(E_m), \quad (8)$$

where the sums \sum' are taken over the reduced spectrum $4 < m < N - 4$ and the reduced norm κ_r and energy E_r are obtained from the numerical values of ρ_m at $t = 2^{22}$ by

$$\kappa_r \equiv \sum'_m \rho_m, \quad E_r \equiv \sum'_m E_m \rho_m. \quad (9)$$

The green curves in Fig. 1 show $\rho_{\text{EQ}}(E_m)$ for the reduced spectrum of $N = 128, 256$, $\beta = 1$, $\gamma = \sigma = 0.01$ (the obtained values of T, μ, κ_r, E_r are given in the caption of Fig. 1). These curves are rather close to the numerical data, but for modes close to the energy boundaries, there are some small but significant deviations and especially for energies in the interval $1 < E_m < 1.8$, the power law based on KZ theory (straight black lines) provides a slightly better fit than the classical equipartition distribution.

Of course, the distribution $\rho_{\text{EQ}}(E_m)$ in (2) can also be viewed as an approximate algebraic decay $1/(E_m + 1)$ at $E_m + 1 \gg \mu$ with the algebraic exponent $s_0 = 1$ as in KZ theory (6). However, there is a fundamental physical difference between the thermal steady state (2) and the turbulence steady state (6): there is no flow between energy scales in (2), while there is a turbulent flow from low to high energies in (6). Thus the empirical fits based on (2) for the numerical data in Fig. 1 can be considered only as some additional empirical descriptions without physical grounds behind.

We show in Fig. 3 the steady-state norm distribution ρ_m for three values of pumping, $\gamma = 0.01; 0.005; 0.0001$, and the same value $\sigma = 0.01$. For the two largest γ values, the pumping is sufficiently strong and the steady-state distribution is rather close to the KZ theory. It is important to note that this steady state is practically independent of the initial values of amplitudes, $C_m(t = 0)$ (for a given fixed realization of the RM \hat{H}). We have verified this point by choosing different random realizations of the initial condition [for the random initial values $C_m(0)$ for $m \leq 8$ with $\kappa(t = 0) = 0.01$] and also localized initial conditions $C_{m_0}(0) = 1$ for a specific mode value m_0 (e.g., with $m_0 = 1$ or $m_0 = N/2$, etc.) and $C_m(0) = 0$ for $m \neq m_0$ [typical initial condition chosen in [12] with $\kappa(t = 0) = 1$]. In all cases and for $N \leq 512$, we obtain essentially the same steady-state distribution at $t = 2^{22}$ with average relative differences $\langle \delta \rho_m / \rho_m \rangle$ of the order of $(1 - 2) \times 10^{-2}$ (for $N = 128, 256$) or $(5 - 10) \times 10^{-2}$ (for $N = 512$). This shows that there a single global chaotic attractor with describes a turbulent flow in the system.

According to Fig. 3, a sufficiently strong pumping with $\gamma = 0.01; 0.005$ leads to a turbulent flow and a steady-state distribution ρ_m , in agreement with the KZ theory. However, at small pumping with $\gamma = 0.0001$, the distribution ρ_m has a very different shape with a fit exponent $s_0 = 2.17 \pm 0.03$. In this case, the total norm is reduced by a factor of 100 with $\kappa = 0.0455$, corresponding to the estimate $\kappa \approx 4\gamma/\sigma$ and a main norm fraction located on pumping modes $m = 1, \dots, 4$, while $\rho_m \sim 10^{-12} - 10^{-6}$ for other $m > 4$. These results show that there is no turbulent flow at a pumping strength below a certain chaos border that corresponds to the spirit of KAM theory. We stress that the notion of chaos border for emergence of the turbulence flow is absent in the theory of KZ turbulence [4]. We do not enter into a deep discussion on the value for the exponent $s_0 \approx 2$ in the nonturbulent regime, but we note that due to RMT properties, the matrix elements V in (3) have approximately the same random values and therefore, based on simple perturbation theory with direct V -matrix element transitions, one can estimate $C_m \sim 1/(E_m - E_1)$ and $\rho_m \sim 1/(E_m - E_1)^2$ (with $E_1 \approx -1$) corresponding to $s_0 = 2$, which is close to the numerical value 2.17.

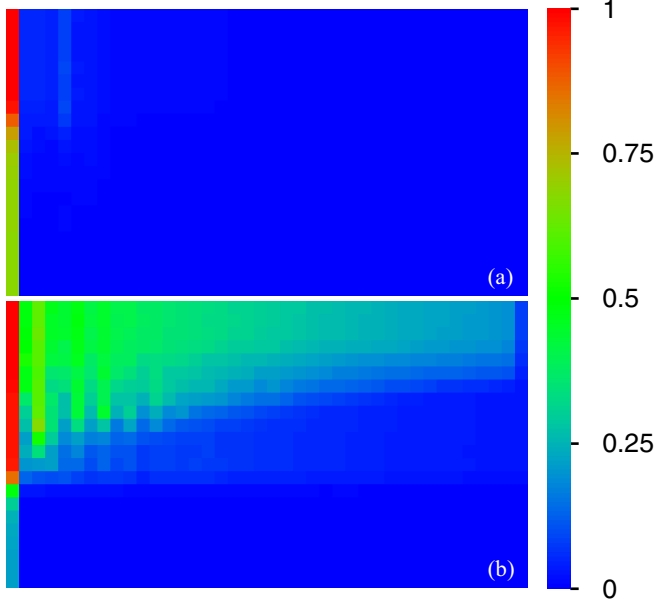


FIG. 4. Color density plot of $\langle \rho_m(t) \rangle$ in the plane $\log_{10}(E_m + 1)$ (x axis) and $\log_2(t)$ (y axis) for the data of Fig. 2 with (a) $\gamma = 0.0001$ and (b) $\gamma = 0.01$ (the other parameters are the same). The values of $\rho_m(t)$ have been obtained from the time average $\rho_m(t) = \langle |C_m(\tau)|^2 \rangle$ for $t/2 \leq \tau \leq t$ with $t = 2^j$ and the index $j = \log_2(t) = 1, 2, \dots, 22$ corresponding to the 22 vertical cells. The 40 horizontal cells correspond to 40 uniform cells in the interval $\log(0.09) \leq \log(E_m + 1) \leq \log(2.1)$ with an additional average of $\rho_m(t) \rightarrow \langle \rho_m(t) \rangle$ for data points (with different E_m) in the same cell. Data points with $E_m + 1 < 0.09$ have been artificially moved to $E_m + 1 = 0.09$ and are taken into account in the average of the first column of cells. The values of the color bar correspond to $(\langle \rho_m(t) \rangle / \rho_{\max})^{1/4}$ with (a) $\rho_{\max} = 0.005058$ and (b) $\rho_{\max} = 0.5051$. The top row of (a) corresponds to the bottom data points of Fig. 2 for $\gamma = 0.0001$ and the top row of (b) corresponds to the top data points of Fig. 2 for $\gamma = 0.01$, both for the last time value $t = 2^{22}$.

The time development of turbulent flow from low to high energies is shown in Fig. 4. At low pumping below the chaos border with $\gamma = 0.0001$, there is no flow to high energies, while for sufficiently strong pumping, a turbulent flow to high energies emerges with a steady-state distribution, in agreement with KZ theory. The turbulent steady-state distribution approximately stabilizes at times $t \approx 2^{18}$.

Finally, in Fig. 5, we show results for the largest studied system size $N = 1024$. Here, at $\gamma = 0.01$, the algebraic decay exponent $s_0 = 2.43 \pm 0.01$ is significantly different from the theoretical value $s_0 = 1$ (6). We attribute this to the fact that the RMT density of states at lowest energies drops significantly and thus, with an increase of matrix size N , the spacing between the lowest E_m values becomes relatively larger compared to those in the middle of the energy band. Thus a higher nonlinearity β is needed to have a dynamical thermalization of these initial eigenmodes. This effect has been discussed in [12] for Hamiltonian dynamics (1). Therefore, a stronger pumping is required to be above a chaos border for KZT. Indeed, the effective nonlinear parameter of the system is $\beta\kappa \sim \beta\gamma/\sigma$ and an increase of γ pumping should drive the system to the KZ turbulent regime. The results of Fig. 5

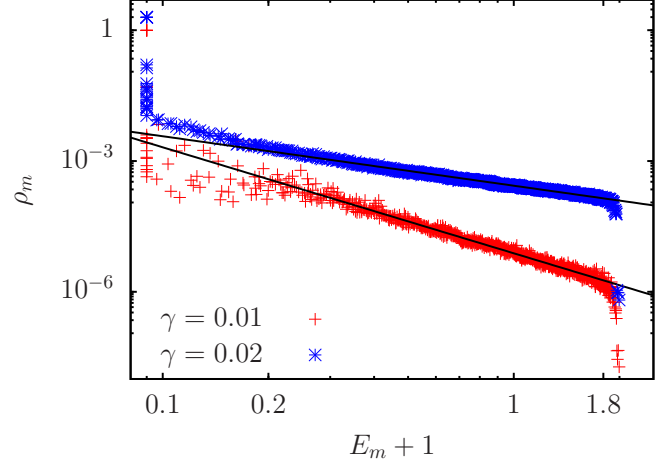


FIG. 5. Same as Fig. 1 for $N = 1024$ and $\gamma = 0.01$ (red +) or $\gamma = 0.02$ (blue *) (the other parameters are the same). The straight lines show the power-law fit $\rho_m = A(1 + E_m)^{-s_0}$ using the fit range $0.2 \leq 1 + E_m \leq 1.8$ with $A = (7.64 \pm 0.04) \times 10^{-6}$, $s_0 = 2.43 \pm 0.01$ (for $\gamma = 0.01$) and $A = (2.713 \pm 0.005) \times 10^{-4}$, $s_0 = 1.134 \pm 0.003$. The total norm is $\kappa = 4.15$ (for $\gamma = 0.01$) and 9.07 (for $\gamma = 0.02$).

confirm that this is the case and at $\gamma = 0.02$ the exponent $s_0 = 1.134 \pm 0.003$ is in good agreement with the KZ theory.

B. Regime of inverse cascade

According to KZ theory [4], there should also be an inverse turbulent cascade of norm flow with the algebraic exponent $x_0 = 2/3$ (7). There have been experiments (see, e.g., [6]) and numerical simulations (see, e.g., [38,39]) of realizations of such an inverse cascade. We try to realize the regime of an inverse cascade (for $\beta = 1$, $\gamma = \sigma = 0.01$, $N = 512$) by performing γ pumping in the same way as before, but placing it either in the middle of the energy band E_m (four modes near $m_0 = N/2$) or in the vicinity of maximal E_m energies (four modes near $m_0 = N - 40$). The absorption is done at both energy boundaries at eight eigenmodes with $m = 1, \dots, 4$ and $m = N - 3, \dots, N$ (using $\gamma_m = -\gamma < 0$ and $\sigma_m = 0$). The initial state is always composed of eight eigenmodes placed around m_0 with random amplitudes and the total initial norm $\kappa(t = 0) \approx 0.01$.

Typical results are shown in Fig. 6. They clearly show an approximately homogeneous norm distribution ρ_m over all energies E_m ; there are more fluctuations for pumping at $m_0 = N - 40$. Clearly, there is no theoretical inverse cascade (7). We explain this fact as follows: a pumping at high m_0 modes leads to a norm transfer at low m modes as is expected from KZ theory. Thus an initially pumped norm $\kappa \approx 4\gamma/\sigma$ is transferred to low energy m modes that leads to a growth of the total norm accumulated in the system. Indeed, the results of Fig. 7 show that in the steady state of the inverse cascade, the total norm $\kappa \approx 48$ is larger by a factor 10 compared to the case of the direct cascade with $\kappa \approx 6$. Thus, for the inverse cascade case, the effective nonlinearity parameter becomes rather large, $\beta\kappa \approx 48$, therefore breaking the regime of weak or moderate nonlinearity. It is possible that one can still try to find a regime where the inverse cascade is present in the

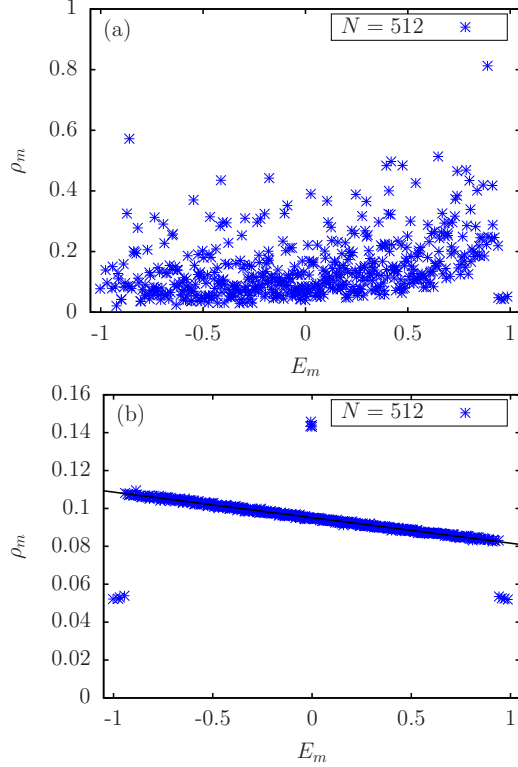


FIG. 6. Distribution ρ_m vs E_m in normal representation for $N = 512$, $\beta = 1$, and $\gamma = \sigma = 0.01$. The values of ρ_m have been obtained from the time average $\rho_m(t) = \langle |C_m(\tau)|^2 \rangle$ for $t/2 \leq \tau \leq t$ with $t = 2^{22}$. Both panels correspond to pumping at $m \approx m_0$ with (a) $m_0 = N - 40 = 472$ or (b) $m_0 = N/2 = 256$, i.e., at $m = m_0 - 2, \dots, m_0 + 1$ and absorption at both boundaries $m = 1, \dots, 4$ and $m = N - 3, \dots, N$. The initial condition corresponds to eight uniform random values $C_m(0)$ at $m \approx m_0$, i.e., $m = m_0 - 4, \dots, m_0 + 3$ and $C_m(0) = 0$ for other m with initial norm $\sum_m |C_m(0)|^2 = 0.01$. The final norm at $t = 2^{22}$ is (a) $\kappa = 74.08$ or (b) $\kappa = 48.52$. The straight line [only for (b)] shows the linear fit $\rho_m = A - B E_m$ using nonpumping and nonabsorption modes with $A = (9.51 \pm 0.01) \times 10^{-2}$ and $B = (1.35 \pm 0.02) \times 10^{-2}$.

RM model of KZT. However, this would require the use of very small γ pumping, which may be below the chaos border. Furthermore, even at small γ values, the total norm should significantly grow in the limit of large system size N , where the weak turbulence approximation is broken. For the case of a direct cascade, there is no such problem since ρ_m is decreasing with growing energy $E_m + 1$ and the total norm κ with related effective nonlinearity parameter $\beta\kappa$ remains bounded to moderate values (see Fig. 7) and the system remains in a regime of weak turbulence where KZ theory is valid.

Here we consider finite-size systems with random matrix couplings between modes. Such a situation corresponds to multimode fibers with a cross section generating chaotic ray dynamics corresponding to a regime of quantum chaos (e.g., D-shape cross section as discussed in [12]); such fibers may have up to a thousand modes. Such systems are rather different from the quasi-infinite sizes used to study the weak turbulence of waves in large systems [5,38,39] (e.g., about a billion modes in [39]). It was shown that at large sizes and a specific pumping, the theoretical inverse cascade can be realized

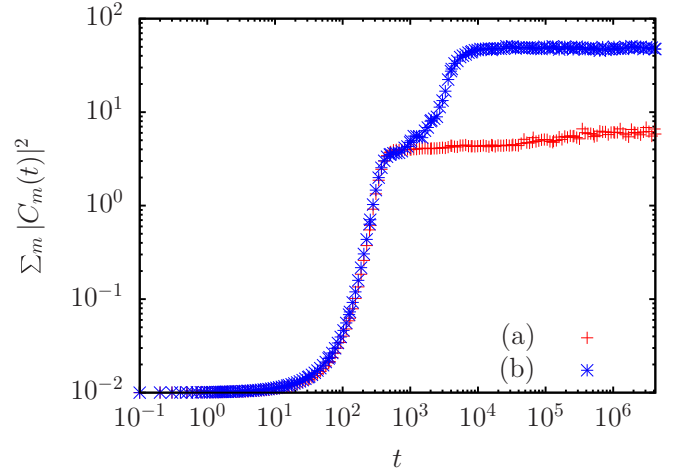


FIG. 7. Time dependence of the (nonaveraged) norm $\sum_m |C_m(t)|^2$ at selected time values for $N = 512$, $\beta = 1$, $\gamma = \sigma = 0.01$. The pumping and absorption parameters are (a) as in Fig. 2 for data points (red +) or (b) as in Fig. 6(b) for data points (blue *). Note that the total norm for times τ in the interval $2^{21} \leq \tau \leq 2^{22}$ is (a) $\kappa = 5.99$ and (b) $\kappa = 48.52$ (see, also, the captions of Figs. 2 and 5).

[39]. We do not exclude that for some specific pumping and very large random matrix sizes, one can find regimes with a theoretical inverse cascade. But for moderate sizes of about a thousand, typical for fibers, we tried various typical forms of pumping that were always leading to a regime of strong nonlinearity. Thus we conclude that the theoretical regime of inverse cascade is hardly reachable for finite-size systems with random matrix interactions between modes, e.g., chaotic fibers. Also, we think that for fibers, it is rather difficult to pump only very high modes.

C. KZT and Anderson localization

In the case of RMM described by Eqs. (1) and (3), the matrix elements V between linear eigenmodes have random amplitudes of the same order between all eigenmodes. It is interesting to consider a case when such couplings have a local structure with transitions only between modes in a certain finite energy range of eigenmodes. As such a model, we consider the discrete Anderson nonlinear Schrödinger equation (DANSE) in a static Stark field,

$$i \frac{\partial \psi_n}{\partial t} = (fn + \varepsilon_n) \psi_n + \beta |\psi_n|^2 \psi_n + (\psi_{n+1} + \psi_{n-1}). \quad (10)$$

Here, ε_n are random on-site energies randomly and homogeneously distributed in the interval $-W/2 \leq \varepsilon_n \leq W/2$, where the hopping takes place only on nearest sites with unit amplitude, and f describes a static Stark field. At $f = \beta = 0$, this system represents the one-dimensional Anderson model with exponentially localized eigenmodes (see, e.g., [40,41]). The localization length at the middle of the energy band is $\ell = 96/W^2$. At moderate nonlinearity with $\beta \sim 1$ and $f = 0$, this Anderson localization is destroyed and an unbounded subdiffusive spreading of the wave packet takes place [42,43]. This spreading is preserved in the presence of a moderate Stark field [44]. In fact, the spreading is subdiffusive such that

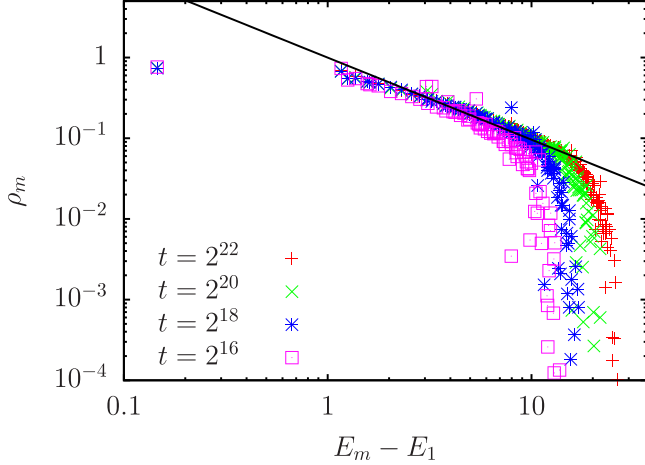


FIG. 8. ρ_m vs $E_m - E_1$ in a double-logarithmic representation for the DANSE model with diagonal shift parameter $f = 0.125$, disorder strength $W = 4$, $N = 256$, $\gamma = \sigma = 0.01$, $\beta = 1$, and pumping, absorption, and initial condition as in Fig. 1. The values of ρ_m have been obtained from the time average $\rho_m(t) = \langle |C_m(\tau)|^2 \rangle$ for $t/2 \leq \tau \leq t$ with $t = 2^{22}$ (red +), $t = 2^{20}$ (green x), $t = 2^{18}$ (blue *), and $t = 2^{16}$ (pink \square). The straight line shows the power-law fit $\rho_m = A(1 + E_m - E_1)^{-s_0}$ using the data for $t = 2^{22}$ and the fit range $0.01(E_N - E_1) \leq (E_m - E_1) \leq 0.5(E_N - E_1)$ with $A = 1.00 \pm 0.04$, $s_0 = 1.02 \pm 0.02$ (and $E_1 = -1.67$, $E_N = 33.42$, $E_N - E_1 = 35.09$). The total norm is $\kappa = 13.86$ (for $t = 2^{16}$), 17.16 (for $t = 2^{18}$), 19.58 (for $t = 2^{20}$), and 21.19 (for $t = 2^{22}$).

the second moment grows as $\langle n^2 \rangle \propto t^\nu$ with the numerical exponent value $\nu \approx 0.3-0.4$ in 1D [42–44]. This value is smaller than $\nu = 0.5$ following from the random phase approximation [45,46]. In [12], it was shown that in such a system of finite size N , the dynamical thermalization takes place at a moderate nonlinearity $\beta \sim 1$ and a moderate Stark field f with the steady-state thermal distribution corresponding to energy equipartition (2).

In the basis of linear eigenmodes of the 1D-Anderson Hamiltonian, the coupling between modes appears only due to the β nonlinearity. In this basis, the time evolution is still described by Eq. (3). However, due to the exponential localization of linear eigenmodes in (10), the matrix elements V are coupling m modes only in a range $\Delta m \sim \ell$, while outside of this range, their amplitude drops exponentially due to Anderson localization.

Due to the above properties, it is natural to use the DANSE model with Stark field for studies of KZT by introducing pumping and absorption in the same way as for the RMM case described above. Another advantage of the model (10) is that due to the presence of the Stark field, the energy band range can be significantly increased compared to the RMT case, where it is fixed to 2.

The results for KZ turbulence in model (10) are presented in Figs. 8 and 9. Here, as in RMM (for the direct cascade), the pumping is done for the four lowest modes $m = 1, \dots, 4$ at $\gamma = \sigma = 0.01$ and absorption is at the highest modes $m = N - 4, \dots, N$. The numerical integration is done in the same way as for the RMM case. We use parameters $\beta = 1$, $W = 4$, and $f = 0.125$ so that at $N = 256$, the energy band width is

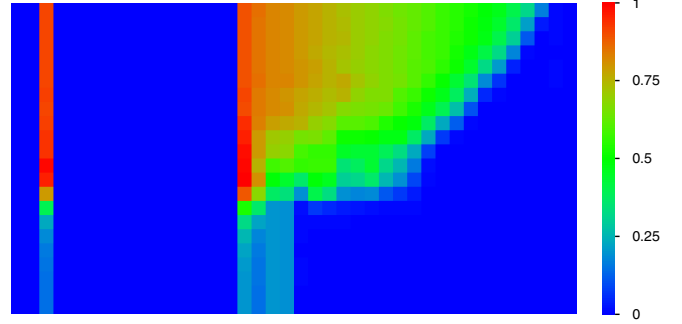


FIG. 9. Color density plot of $\langle \rho_m(t) \rangle$ in the plane $\log(E_m - E_1)$ (x axis) and $\log_2(t)$ (y axis) for the DANSE model using the data of Fig. 8 (similar style as in Fig. 4). The values of $\rho_m(t)$ have been obtained from the time average $\rho_m(t) = \langle |C_m(\tau)|^2 \rangle$ for $t/2 \leq \tau \leq t$, with $t = 2^j$ and the index $j = \log_2(t) = 1, 2, \dots, 22$ corresponding to the 22 vertical cells. The 40 horizontal cells correspond to 40 uniform cells in the interval $\log(0.1) \leq \log(E_m - E_1) \leq \log(1.1 \times E_N)$ (same energy interval shown in Fig. 8), with an additional average of $\rho_m(t) \rightarrow \langle \rho_m(t) \rangle$ for data points (with different E_m) in the same cell. The column 3 with first nonzero (nonblue) values corresponds to the data for E_2 . The values of the color bar correspond to $(\langle \rho_m(t) \rangle / \rho_{\max})^{1/4}$, with $\rho_{\max} = 1.072$. The top 1,3,5,7 rows correspond to the data points of Fig. 8 for $t = 2^{22}, 2^{20}, 2^{18}, 2^{16}$, respectively.

approximately 32, which is larger by a factor of 16 compared to RMM. At such parameters, the localization length $\ell = 16$ is significantly smaller than the lattice size N . The time evolution of the norm distribution ρ_m is shown in Fig. 8 at four discrete time values. The color density plot of Fig. 9 shows the same data as Fig. 8, but for all times $2 \leq t \leq 2^{22}$ in the same style as Fig. 4 for the RMM. It takes a rather long time to reach the absorption boundary due to the slow subdiffusive spreading in the DANSE model. However, with time, the KZT profile (6) stabilizes as well as the total norm growth. In the steady state, we find the algebraic decay exponent $s_0 = 1.02 \pm 0.02$ that is practically equal to the theoretical value $s_0 = 1$. We think that an increase of the energy band width allows one to obtain a more exact value of s_0 .

We note that previously, an interplay between the KZ turbulence process and the Anderson localization has been discussed in [47,48]. It was found that the KZ turbulent flow to high energies can be stopped by the Anderson localization and KAM integrability. However, in the models considered in [47,48], the energy pumping at low energy modes was chosen to be unitary so that the total norm was conserved. Due to this, the nonlinear interaction was kept on a fixed level. In the case of model (10) considered here, the pumping is changing the total norm so that the system itself relaxes to a steady state with a self-determined total norm. Therefore, in such a case, the Anderson localization cannot stop the KZ turbulent flow which propagates to the highest available energies. However, as with the RMM case (see Figs. 3 and 4), a weak pumping in the DANSE model with Stark field (10) keeps the system in the KAM integrable regime below the chaos border and there is no turbulent flow to high energies.

Finally, we note that for the case of the DANSE model (10) with $f = 0$ and with the pumping done in the original

n basis, we find that the total norm is growing and the wave packet spreads over the whole system size. Due to this, the norm growth of such a case is not of physical interest.

V. DISCUSSION

In this work, we introduced and studied a random matrix model of the Kolmogorov-Zakharov turbulence. The model evolution is described by purely dynamical equations of motion without any external thermal bath or noise. As shown in [12], in the absence of dynamical pumping and dissipation, the Hamiltonian chaotic dynamics leads to a thermal equilibrium distribution with energy equipartition over energies of linear modes. Thus the dynamical evolution produces an emergence of a thermal law description of statistical mechanics. The introduction of energy and norm pumping at low energy modes and dissipation at high energy modes (also described by dynamical equations only) leads to a global chaotic attractor which describes an energy flow from low to high energies corresponding to the KZ theory concept [4]. This direct turbulent flow is characterized by an algebraic decay of norm from low to high energies, with the exponent being close to the KZT theoretical value ($s_0 = 1$). Thus the studied system can be viewed as a purely dynamical model of KZ turbulence. At the same time, we show that in this model, a turbulent flow appears only at a pumping strength that is above a certain chaos border related to KAM integrability of motions in the case of very weak nonlinearity. We also show that the RMM case of KZT is rather generic and, even when linear eigenmodes are exponentially localized in the lattice basis due to Anderson localization, we still have the direct

turbulent cascade well described by KZ theory when pumping is above a certain chaos border.

However, in the RMM case, we do not find a regime of the inverse KZ cascade. We attribute this to a strong norm growth driving the system to a strongly nonlinear regime when the approach of weak turbulence and weak nonlinearity is not applicable.

We note that the dynamical thermalization has been recently observed in the experiments with multimode fibers (see, e.g., [30–34]) and we assume that the RMM system discussed here for the KZ turbulence can be realized in fibers with a cross section of a chaotic 2D billiard. Such quantum billiards have many properties of quantum chaos [16,17] that are similar to the RMT case studied here. As discussed in [12], we think that a most optimal billiard section of fiber is a D-shape one (a circle with cut), where the classical dynamics is known to be chaotic (see, e.g., [49]). We expect that in multimode fibers, the KZT regime can be realized by a continuous laser pumping of low energy modes, while the light at high energy modes will escape from a fiber due to high angle collisions with the fiber perimeter, thus leading to a stationary KZT flow from low to high energies.

ACKNOWLEDGMENTS

This work has been partially supported through the NANOX Grant No. ANR-17-EURE-0009 in the framework of the Programme Investissements d’Avenir (project MTD-INA). This work was granted access to the HPC resources of CALMIP (Toulouse) under the allocation 2023-P0110.

-
- [1] A. N. Kolmogorov, The local structure of turbulence in an incompressible liquid for very large Reynolds numbers, *Dokl. Akad. Nauk SSSR* **30**, 299 (1941); Dissipation of energy in the locally isotropic turbulence, **32**, 19 (1941) [*Proc. R. Soc. Ser. A* **434**, 15 (1991)].
 - [2] A. M. Obukhov, On energy distribution in the spectrum of a turbulent flow, *Izv. AN SSSR Ser. Geogr. Geofiz.* **5**, 453 (1941).
 - [3] V. E. Zakharov and N. N. Filonenko, Weak turbulence of capillary waves, *J. Appl. Mech. Tech. Phys.* **8**, 37 (1971).
 - [4] V. E. Zakharov, V. S. L’vov, and G. Falkovich, *Kolmogorov Spectra of Turbulence* (Springer-Verlag, Berlin, 1992).
 - [5] S. Nazarenko, *Wave Turbulence* (Springer-Verlag, Berlin, 2011).
 - [6] S. Nazarenko and S. Lukaschuk, Wave turbulence on water surface, *Annu. Rev. Condens. Matter Phys.* **7**, 61 (2016).
 - [7] S. Galtier, *Physics of Wave Turbulence* (Cambridge University Press, Cambridge, UK, 2023).
 - [8] V. Arnold and A. Avez, *Ergodic Problems of Classical Mechanics* (Benjamin, New York, 1968).
 - [9] I. P. Cornfeld, S. V. Fomin, and Ya. G. Sinai, *Ergodic Theory* (Springer-Verlag, New York, 1982).
 - [10] B. V. Chirikov, A universal instability of many-dimensional oscillator systems, *Phys. Rep.* **52**, 263 (1979).
 - [11] A. J. Lichtenberg and M. A. Lieberman, *Regular and Chaotic Dynamics* (Springer, Berlin, 1992).
 - [12] K. M. Frahm and D. L. Shepelyansky, Nonlinear perturbation of random matrix theory, *Phys. Rev. Lett.* **131**, 077201 (2023).
 - [13] E. P. Wigner, Random matrices in physics, *SIAM Rev.* **9**, 1 (1967).
 - [14] M. L. Mehta, *Random Matrices* (Elsevier, Amsterdam, 2004).
 - [15] T. Guhr, A. Müller-Groeling, and H. A. Weidenmüller, Random matrix theories in quantum physics: Common concepts, *Phys. Rep.* **299**, 189 (1998).
 - [16] O. Bohigas, M.-J. Giannoni, and C. Schmit, Characterization of chaotic quantum spectra and universality of level fluctuation laws, *Phys. Rev. Lett.* **52**, 1 (1984).
 - [17] F. Haake, *Quantum Signatures of Chaos* (Springer, Berlin, 2010).
 - [18] L. D. Landau and E. M. Lifshitz, *Statistical Physics* (Wiley, New York, 1976).
 - [19] E. Fermi, J. Pasta, and S. Ulam, Studies of nonlinear problems, Los Alamos Report LA-1940 (1955); published later in E. Fermi *Collected Papers*, edited by E. Serge, Vol. 2, 491 (University of Chicago Press, Chicago, IL, 1965); see, also, the historical overview in T. Dauxois, Fermi, Pasta, Ulam and a mysterious lady, *Phys. Today* **61**, 55 (2008).
 - [20] C. S. Gardner, J. M. Greene, M. D. Kruskal, and R. M. Miura, Method for solving the Korteweg–de Vries equation, *Phys. Rev. Lett.* **19**, 1095 (1967).
 - [21] V. E. Zakharov and A. B. Shabat, Interaction between solitons in a stable medium, *Sov. Phys. JETP* **37**, 823 (1973).

- [22] M. Toda, Studies of a nonlinear lattice, *Phys. Rep.* **18**, 1 (1975).
- [23] L. D. Landau and E. M. Lifshitz, *Fluid Mechanics* (Pergamon Press, New York, 1989).
- [24] T. V. Laptjeva, A. A. Tikhomirov, O. I. Kanakov, and M. V. Ivanchenko, Anderson attractors in active arrays, *Sci. Rep.* **5**, 13263 (2015).
- [25] G. Rollin, J. Lages, and D. L. Shepelyansky, Random lasing from Anderson attractors, *Phys. Rev. A* **105**, 053506 (2022).
- [26] B. V. Chirikov and D. L. Shepelyanskii, Dynamics of some homogeneous models of classical Yang-Mills fields, *Sov. J. Nucl. Phys.* **36**, 908 (1982).
- [27] D. L. Shepelyansky, Delocalization of quantum chaos by weak nonlinearity, *Phys. Rev. Lett.* **70**, 1787 (1993).
- [28] I. García-Mata and D. L. Shepelyansky, Delocalization induced by nonlinearity in systems with disorder, *Phys. Rev. E* **79**, 026205 (2009).
- [29] A. Ramos, L. Fernandez-Alcazar, T. Kottos, and B. Shapiro, Optical phase transitions in photonic networks: A spin-system formulation, *Phys. Rev. X* **10**, 031024 (2020).
- [30] K. Baudin, A. Fusaro, K. Krupa, J. Garnier, S. Rica, G. Millot, and A. Picozzi, Classical Rayleigh-Jeans condensation of light waves: Observation and thermodynamic characterization, *Phys. Rev. Lett.* **125**, 244101 (2020).
- [31] N. Berti, K. Baudin, A. Fusaro, G. Millot, A. Picozzi, and J. Garnier, Interplay of thermalization and strong disorder: Wave turbulence theory, numerical simulations, and experiments in multimode optical fibers, *Phys. Rev. Lett.* **129**, 063901 (2022).
- [32] E. V. Podivilov, F. Mangini, O. S. Sidelnikov, M. Ferraro, M. Gervaziev, D. S. Kharenko, M. Zitelli, M. P. Fedoruk, S. A. Babin, and S. Wabnitz, Thermalization of orbital angular momentum beams in multimode optical fibers, *Phys. Rev. Lett.* **128**, 243901 (2022).
- [33] F. Mangini, M. Gervaziev, M. Ferraro, D. S. Kharenko, M. Zitelli, Y. Sun, V. Couderc, E. V. Podivilov, S. A. Babin, and S. Wabnitz, Statistical mechanics of beam self-cleaning in GRIN multimode optical fibers, *Opt. Express* **30**, 10850 (2022).
- [34] K. Baudin, J. Garnier, A. Fusaro, N. Berti, C. Michel, K. Krupa, G. Millot, and A. Picozzi, Observation of light thermalization to negative-temperature Rayleigh-Jeans equilibrium states in multimode optical fibers, *Phys. Rev. Lett.* **130**, 063801 (2023).
- [35] M. Mulansky, K. Ahnert, A. Pikovsky, and D. L. Shepelyansky, Strong and weak chaos in weakly nonintegrable many-body Hamiltonian systems, *J. Stat. Phys.* **145**, 1256 (2011).
- [36] D. L. Shepelyansky, Low energy chaos in the Fermi-Pasta-Ulam problem, *Nonlinearity* **10**, 1331 (1997).
- [37] X.-Y. Hu and V. Rosemhaus, The random coupling model of turbulence as a classical SYK model, *Phys. Rev. E* **108**, 054132 (2023).
- [38] S. Y. Annenkov and V. I. Shrira, Direct numerical simulation of downshift and inverse cascade for water wave turbulence, *Phys. Rev. Lett.* **96**, 204501 (2006).
- [39] Y. Zhu, B. Semisalov, G. Krstulovic, and S. Nazarenko, Direct and inverse cascades in turbulent Bose-Einstein condensates, *Phys. Rev. Lett.* **130**, 133001 (2023).
- [40] B. Kramer and A. MacKinnon, Localization: Theory and experiment, *Rep. Prog. Phys.* **56**, 1469 (1993).
- [41] F. Evers and A. D. Mirlin, Anderson transitions, *Rev. Mod. Phys.* **80**, 1355 (2008).
- [42] A. S. Pikovsky and D. L. Shepelyansky, Destruction of Anderson localization by a weak nonlinearity, *Phys. Rev. Lett.* **100**, 094101 (2008).
- [43] T. V. Laptjeva, M. I. Ivanchenko, and S. Flach, Nonlinear lattice waves in heterogeneous media, *J. Phys. A: Math. Theor.* **47**, 493001 (2014).
- [44] I. García-Mata and D. L. Shepelyansky, Nonlinear delocalization on disordered Stark ladder, *Eur. Phys. J. B* **71**, 121 (2009).
- [45] D. Basko, Kinetic theory of nonlinear diffusion in a weakly disordered nonlinear Schrodinger chain in the regime of homogeneous chaos, *Phys. Rev. E* **89**, 022921 (2014).
- [46] S. Nazarenko, A. Soffer, and M.-B. Tran, On the wave turbulence theory for the nonlinear Schrodinger equation with random potentials, *Entropy* **21**, 823 (2019).
- [47] D. L. Shepelyansky, Kolmogorov turbulence, Anderson localization and KAM integrability, *Europhys. J. B* **85**, 199 (2012).
- [48] L. Ermann, E. Vergini, and D. L. Shepelyansky, Kolmogorov turbulence defeated by Anderson localization for a Bose-Einstein condensate in a Sinai-oscillator trap, *Phys. Rev. Lett.* **119**, 054103 (2017).
- [49] K. Kim, S. Bittner, Y. Jin, Y. Zeng, Q. J. Wang, and H. Cao, Impact of cavity geometry on microlaser dynamics, *Phys. Rev. Lett.* **131**, 153801 (2023).